Homonuclear ionizing collisions of laser-cooled metastable helium atoms

R. J. W. Stas, J. M. McNamara, W. Hogervorst, and W. Vassen
Laser Centre, Vrije Universiteit, De Boelelaan 1081, 1081 HV Amsterdam, The Netherlands
(Received 5 September 2005; published 14 March 2006)

We present a theoretical and experimental investigation of homonuclear ionizing collisions of laser-cooled metastable ($2\,^3S_1$) helium atoms, considering both the fermionic ^{3}He and bosonic ^{4}He isotopes. The theoretical description combines quantum threshold behavior, Wigner's spin-conservation rule, and quantum-statistical symmetry requirements in a single-channel model, complementing a more complete close-coupling theory that has been reported for collisions of metastable ^{4}He atoms. The model is supported with measurements (in the absence of light fields) of ionization rates in magneto-optically trapped samples that contain about 3×10^8 atoms of a single isotope. The ionization rates are determined from measurements of trap loss due to light-assisted collisions combined with comparative measurements of the ion production rate in the absence and presence of trapping light. Theory and experiment show good agreement.

DOI: 10.1103/PhysRevA.73.032713 PACS number(s): 34.10.+x, 34.50.Fa, 34.50.Rk, 34.20.Cf

I. INTRODUCTION

Soon after the first demonstration of laser cooling of neutral atoms, it was recognized that collisions between atoms have a profound effect on the physics of laser-cooled atomic gases [1]. Light-assisted collisions and other inelastic collision processes constitute loss channels that limit the attainable atomic densities in laser-cooled samples. The magneto-optical trap (MOT) was found to be a versatile tool for accurate investigation of these inelastic collisions [2], which occur at collision energies of 10^{-7} eV in samples with temperatures around 1 mK. Measuring loss rates from the trap, the cross section for inelastic collisions can be determined with great precision [3]. Experiments as well as theoretical work, almost exclusively carried out in alkali-metal systems, have provided a wealth of information on cold collisions [3], which play a critical role in many research areas that have emerged since the advent of laser cooling [4].

Laser-cooled helium atoms in the metastable $2\,^3S_1$ state, denoted He*, provide unique opportunities to study cold ionizing collisions,

$$\mathrm{He}^* + \mathrm{He}^* \rightarrow \mathrm{He} + \mathrm{He}^+ + e^- \quad (PI), \tag{1}$$

$$\mathrm{He}^* + \mathrm{He}^* \rightarrow \mathrm{He}_2^+ + e^- \quad (AI), \tag{2}$$

where PI stands for Penning ionization and AI for associative ionization. The simple structure of the helium atom allows for theoretical exercises that are relatively uncomplicated, while experiments profit by the possibility of direct detection of ions with charged-particle detectors. Furthermore, large numbers of atoms ($\sim3\times10^8$), either ^{3}He* or ^{4}He*, can be confined in a MOT [5], so that differences between collisions of fermionic (^{3}He*) and bosonic atoms (^{4}He*) can be investigated.

In this paper, a theoretical and experimental investigation of homonuclear ionizing collisions of ^{3}He* and ^{4}He* atoms is presented, with particular regard to isotopic differences in ionizing collisions. The theoretical model is a single-channel calculation of the ionization cross section and rate coefficient for ionizing collisions, which can be applied to both isotopes. In the experiments, magneto-optically trapped samples of ^{3}He* or ^{4}He* atoms are investigated and ionization rates are measured with a microchannel plate (MCP) detector. The measurements are performed in the absence of trapping light, as optical excitation by near-resonant light alters the dynamics of cold collisions [3,6], thereby strongly enhancing the ionization rate [7–14].

Combining theory and experiment, the present work extends previous studies and may be used to unravel inconsistencies in reported experimental results [15]. The transparent theoretical model complements close-coupling calculations that have been performed for collisions of ^{4}He* atoms [15–17]. Other studies of ^{4}He* collisions provide little detail [8,18] or focus exclusively on collisions of spin-polarized atoms (to investigate the feasibility of Bose-Einstein condensation) [19,20], while another theoretical study, which applies to both ^{3}He* and ^{4}He* collisions [11], is based on questionable assumptions. The extensive description of the experimental procedure and exhaustive explanation of the data analysis procedure provides clear insight into the origin of experimental ionization rate coefficients and can be used to evaluate other experimental studies of ionizing collisions of He* atoms [8,10,11,21].

The paper is organized as follows. Section II presents the theoretical model for homonuclear ionizing collisions of laser-cooled helium isotopes. First a simplified expression for the ionization cross section is derived (Sec. II A). Using an effective molecular potential (Sec. II B), partial-wave ionization cross sections are derived from numerical solutions of the one-dimensional Schrödinger equation (Sec. II C) and the corresponding partial-wave ionization rate coefficients are calculated (Sec. II D). Quantum-statistical symmetry requirements are taken into account (Sec. II E) to derive the rate coefficient for samples of either ^{3}He* or ^{4}He* atoms with a given population of magnetic sublevels. Finally, the results are compared with other theoretical results (Sec. II F). Section III describes the measurement of the ionization rate coefficients in laser-cooled samples of ^{3}He* or ^{4}He* atoms. Subdividing loss mechanisms into ionizing and nonionizing contributions, and distinguishing between linear and qua-

dratic trap loss, an overview of trap loss mechanisms occurring in our He^* samples is presented and estimates of ionization and trap loss rates are derived (Sec. III A). It is shown that ionization rates can be deduced from trap loss measurements if the contribution of ionizing mechanisms to trap loss is determined. Measurements of trap loss due to light-assisted collisions are presented (Sec. III B). Comparative ion production rate measurements in the absence and presence of trapping light are used to determine the ionization rate coefficients in the absence of light fields (Sec. III C). Finally, the results are compared with our theoretical predictions (Sec. III D). Section IV presents a discussion of the theoretical and experimental results, as well as conclusions and prospects.

II. THEORETICAL MODEL

The ionizing collisions of Eqs. (1) and (2) are highly exothermic, as the internal energy of two He^* atoms exceeds the 24.6 eV ionization energy of the He atom by more than 15 eV. As differences between PI and AI are unimportant for the work presented here (the reaction mechanisms have been discussed in detail in Ref. [22]), we will not distinguish between them and use the term PI to denote both processes.

The interaction that drives the autoionizing transitions of Eqs. (1) and (2) is of an electrostatic nature [22], so that it only induces transitions between molecular states of equal total electronic spin. Therefore, ionization rates associated with the reactions of Eqs. (1) and (2) depend on the total spin states on the reactant and product sides of the reaction formulas. For both reactions, the reactants carry an electronic spin of $s=1$ and can form total spin states with $S=0,1$ or 2, while the products, carrying $s=\frac{1}{2}$ (except for ground-state helium, which carries no electronic spin), can only form states with $S=0$ or 1. Clearly, total electronic spin can only be conserved if $S=0$ or 1, and a PI reaction with $S=2$ would involve a violation of spin conservation. It has been shown [19,20] that a very weak spin-dipole magnetic interaction can induce spin flips and mediate PI in collisions of He^* atoms with $S=2$. The corresponding ionization rate is four orders of magnitude smaller than those of collisions with $S=0$ and 1, for which total electronic spin is conserved [23]. The strong suppression of PI by spin conservation is known as Wigner's spin-conservation rule [24] and has been observed for He^* collisions in a gas discharge [25], a laser-cooled sample [21], and a Bose-Einstein condensate [26–28]. In heavier metastable rare-gas systems, Wigner's spin-conservation rule does not apply [29], and polarized samples can be used for the investigation of quantum-statistical effects in ionizing collisions [30,31].

At the millikelvin temperatures of a laser-cooled sample of He^* atoms, collisions occur at relative kinetic energies $E=\mu v_r^2/2\approx 10^{-7}$ eV, where $\mu=m/2$ is the reduced mass of the colliding atoms (with m the mass of the He atom) and v_r is the relative velocity between the atoms. As the de Broglie wavelength of atomic motion $\Lambda=h/\mu v_r\approx 250a_0$ (with h Planck's constant) is much larger than the typical scale of the interatomic potential, collisions are dominated by quantum threshold behavior [18,32–35]. In this case, the collision process can be described conveniently using the partial-wave method [36]: the ionization cross section, written as a sum of partial-wave contributions,

$$\sigma^{(\mathrm{ion})}=\sum_{\ell}\sigma_{\ell}^{(\mathrm{ion})}, \tag{3}$$

is dominated by only a few partial waves ℓ. For inelastic exothermic collisions, such as Penning ionizing collisions, the quantum threshold behavior of the ℓth partial cross section is given by [3,18,34]

$$\sigma_{\ell}^{(\mathrm{ion})}\propto k^{2\ell-1} \quad \text{if } k\to 0. \tag{4}$$

Here, $k=(2\mu E/\hbar^2)^{1/2}$ is the wave vector of the asymptotic relative motion of the colliding atoms, with $\hbar=h/2\pi$. In a sufficiently cold sample of He^* atoms, the cross section for Penning ionizing collisions is dominated by the s-wave contribution $\sigma_0^{(\mathrm{ion})}$, which diverges as $1/k$ if $k\to 0$ [32]. Elastic collisions have very different threshold properties: the cross section $\sigma_0^{(\mathrm{elas})}$ approaches a nonvanishing constant, $\sigma_1^{(\mathrm{elas})}\propto k^4$ and $\sigma_{\ell>1}^{(\mathrm{elas})}\propto k^6$, if $k\to 0$ [3,37].

For collisions of He^* atoms, the partial-wave cross section $\sigma_{\ell}^{(\mathrm{ion})}$ can be derived from the solution of an effective one-dimensional potential scattering problem (Secs. II A–II D). Restrictions imposed by the symmetry postulate on the partial waves that contribute to the cross section of Eq. (3) can be taken into account thereafter (Sec. II E).

A. Ionization cross section

From a semiclassical point of view, two events can be distinguished in the process of a cold ionizing collision of two He^* atoms: (1) elastic scattering of the atoms by the interaction potential $V(R)$, with R the internuclear distance, and (2) Penning ionization that occurs when the two electron clouds start to overlap [22]. As collision energies are small, the elastic scattering occurs at a relatively large internuclear distance $R\gtrsim 100a_0$. For partial waves $\ell>0$, the radial wave function $u_{k\ell}(R)$ [cf. Eq. (6)] is scattered by the centrifugal barriers, while scattering for $\ell=0$ takes place at the internuclear distance where the local de Broglie wavelength $\Lambda(R)=h/\{2\mu[E-V(R)]\}^{1/2}$ becomes comparable to the size of the potential, i.e., $d\Lambda(R)/dR\approx 1$ [18,34]. As the electron clouds of both atoms start to overlap at small internuclear distance $R\approx 5a_0$ [38], the elastic scattering process can be considered to precede the inelastic process of ionization.

In the spirit of Ref. [31], we assume that the two subsequent processes can be treated separately. As PI is a strong inelastic exothermic process, we can write the ionization cross section for collisions with total electronic spin S as [31]

$${}^{(2S+1)}\sigma^{(\mathrm{ion})}=\frac{\pi}{k^2}\sum_{\ell}(2l+1)\,{}^{(2S+1)}P_{\ell}^{(\mathrm{tun})}\,{}^{(2S+1)}P^{(\mathrm{ion})}, \tag{5}$$

where ${}^{(2S+1)}P_{\ell}^{(\mathrm{tun})}$ is the probability for the atoms to reach a small internuclear distance, and ${}^{(2S+1)}P^{(\mathrm{ion})}$ is the probability for ionization to occur at that place. As total spin S is strongly conserved during ionization, ${}^{(2S+1)}P^{(\mathrm{ion})}$ is very small ($\ll 1$) for collisions that violate Wigner's spin-

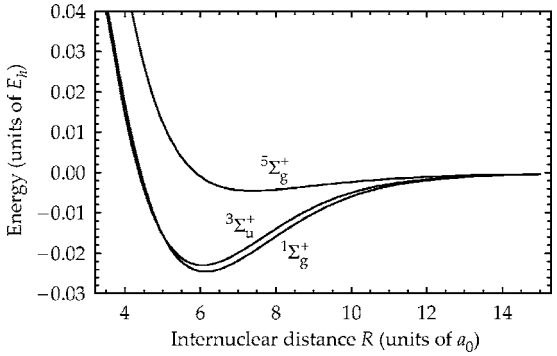

FIG. 1. *Ab initio* potential energy curves in atomic units, calculated for $^4He^*$ by Müller *et al.* [38].

conservation rule. Here, we neglect ionizing collisions with $S=2$ and assume that $^5P^{(\mathrm{ion})}=0$. As ionization occurs with essentially unit probability for the other spin states (Müller *et al.* [38] report an ionization probability of 0.975), we set $^1P^{(\mathrm{ion})}=^3P^{(\mathrm{ion})}=1$.

The calculation of cross sections $^{(2S+1)}\sigma^{(\mathrm{ion})}$ is reduced to the determination of partial-wave tunneling probabilities $^{(2S+1)}P_\ell^{(\mathrm{tun})}$. The energy dependence of the probabilities $^{(2S+1)}P_\ell^{(\mathrm{tun})}$ gives rise to an energy-dependent $^{(2S+1)}\sigma^{(\mathrm{ion})}$, which displays the quantum threshold behavior of the inelastic collisions of Eq. (4). To calculate $^{(2S+1)}P_\ell^{(\mathrm{tun})}$, we need to consider the interaction potential of the colliding atoms.

B. Effective potential

As the helium atom, with only two electrons and a nucleus, has a relatively simple structure, interatomic potentials can be calculated with high accuracy. Figure 1 shows the short-range part ($3.5a_0<R<14.0a_0$) of the potential curves for two metastable $2\,^3S_1$ helium atoms obtained from Müller *et al.* [38]. The curves are the result of *ab initio* calculations in the Born-Oppenheimer approximation, where total electronic spin S is a good quantum number. The possible values $S=0$, 1, and 2 correspond to a singlet, triplet, and quintet potential [$^1V(R)$, $^3V(R)$, and $^5V(R)$], respectively. In Fig. 1, the curves are labeled in Hund's case (a) notation $^{2S+1}\Lambda^{\pm}_{g/u}$, where $\Lambda=|M_L|$ with M_L the quantum number of the projection of the total electronic orbital angular momentum onto the internuclear axis of the molecule, g/u stands for gerade or ungerade, i.e., positive or negative symmetry under inversion of all electronic coordinates of the molecule, and $\pm$ indicates positive or negative symmetry under reflection through a plane including the internuclear axis [39]. As both electrons of the He^* atom are in s states, colliding atom pairs can only have zero total orbital angular momentum, indicated by $\Lambda=\Sigma$.

The potentials can be extended to large internuclear distance using a calculation of the dispersion interaction of two He^* atoms; for a multipole expansion $-C_6/R^6-C_8/R^8-C_{10}/R^{10}$, dispersion coefficients $C_6=3276.680$ a.u., $C_8=210\,566.55$ a.u., and $C_{10}=21\,786\,760$ a.u. have been reported [40,41]. Here, we construct potentials valid for $R>3.5a_0$ by fitting the short-range potential curves of Fig. 1 smoothly onto the long-range dispersion interaction around $20a_0$ by interpolation using a cubic spline fitted to $R^6\times{}^{(2S+1)}V(R)$.

The elastic scattering for collisions with $S=0$ and 1 is governed by potentials $^1V(R)$ and $^3V(R)$, respectively. Within the framework of the partial-wave method, potential scattering by $^{(2S+1)}V(R)$ is described by the radial wave equation [42]

$$-\frac{\hbar^2}{2\mu}\frac{d^2}{dR^2}u_{k\ell}(R)+\left(\frac{\hbar^2\,\ell\,(\ell+1)}{2\mu R^2}+{}^{(2S+1)}V(R)-E\right)u_{k\ell}(R)=0, \tag{6}$$

where ℓ is the quantum number of the relative angular momentum and $u_{k\ell}(r)$ is the radial wave function. Equation (6) can be interpreted as a one-dimensional Schrödinger equation ($R\geqslant 3.5a_0$), describing the potential scattering of a particle of mass μ by the effective potential

$${}^{(2S+1)}V_\ell(R)={}^{(2S+1)}V(R)+\frac{\hbar^2\,\ell\,(\ell+1)}{2\mu R^2}, \tag{7}$$

where the second term is the well-known centrifugal potential.

To calculate the probability $^{(2S+1)}P_\ell^{(\mathrm{tun})}$ of atom pairs to reach the distance where ionization occurs, we modify the effective potential curves to simulate the ionization process. We set the curves to a constant value for small internuclear distances, and extend the range of R to negative values [20,31],

$${}^{(2S+1)}\tilde{V}_\ell(R)=\begin{cases}{}^{(2S+1)}V_\ell(R_0), & R\leqslant R_0,\\ {}^{(2S+1)}V_\ell(R), & R>R_0,\end{cases} \tag{8}$$

where $R_0=6.1a_0$ is chosen to be the location of the potential curve minimum. In this way, we avoid reflections of the radial wave function from artificial features of the potential energy curve at R_0. Modeling the interatomic interaction by $\tilde{V}_\ell(R)$, potential scattering is described by the one-dimensional Schrödinger equation ($-\infty<R<\infty$)

$$-\frac{\hbar^2}{2\mu}\frac{d^2}{dR^2}u_{k\ell}(R)+[{}^{(2S+1)}\tilde{V}_\ell(R)-E]u_{k\ell}(R)=0, \tag{9}$$

and ionizing collisions correspond to the transmission of the relative particle to $R<0$: for atoms that reach the region of small R, where ionization takes place, the corresponding relative particle will propagate freely to $R=-\infty$ and never reflect back to $R>R_0$. The disappearance of the particle to $R<0$ results in a loss of probability flux.

Figure 2 shows plots of $\tilde{V}_0(R)$, $\tilde{V}_1(R)$, and $\tilde{V}_2(R)$ for homonuclear collisions of both $^3He^*$ and $^4He^*$ atoms, where we have used the atomic mass $m=3.016\,03$ u for $^3He^*$ and $m=4.0026$ u for $^4He^*$, with 1 u=1822.89 a.u. For an atomic sample with a thermal velocity distribution with temperature T, the mean collision energy is given by $\langle E\rangle=\frac{3}{2}k_BT$; this relation is used to express the potentials in units of temperature.

The barriers formed by centrifugal potentials with $\ell=1$ and 2 are five orders of magnitude smaller than the potential

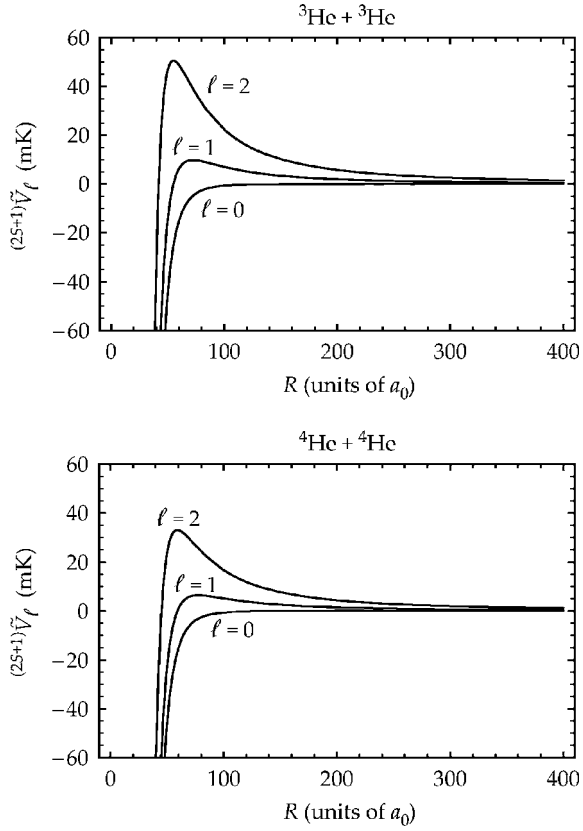

FIG. 2. Potentials $^{(2S+1)}\tilde{V}_\ell(R)$ with centrifugal barriers. The centrifugal interaction is smaller than the short-range attraction by five orders of magnitude.

energy associated with the short-range attraction of the colliding atoms. However, even the lowest barrier, with $\ell=1$, is large compared to the temperature of 1 mK that is typical of samples of laser-cooled He^* atoms, and the barrier heights increase with increasing ℓ. Therefore, the probability $^{(2S+1)}P_\ell^{(\mathrm{tun})}$ is small for $\ell=1$ and decreases rapidly for larger values of ℓ.

C. Effective potential scattering problem

The probability of transmission through a barrier in a potential can be calculated from the stationary states associated with the potential [36]. To calculate the probability for transmission to $R<0$ in potential $^{(2S+1)}\tilde{V}_\ell(R)$, we consider stationary states that correspond to the sum of an incident and a reflected wave for $R\gg 1$, and a single transmitted wave for $R\leqslant R_0$. The transmission probability $^{(2S+1)}P_\ell^{(\mathrm{tun})}$ can be written as [36]

$$^{(2S+1)}P_\ell^{(\mathrm{tun})}=\frac{J_{\mathrm{tr}}}{J_{\mathrm{in}}}, \tag{10}$$

where J_{in} and J_{tr} are the probability fluxes associated with incident and transmitted plane waves, respectively. Numerical methods are used to calculate $^{(2S+1)}P_\ell^{(\mathrm{tun})}$, for $\ell=0,1,2$ and a range of collision energies E.

For a typical collision energy $E=9.5\times10^{-9}$ a.u. $\left(E/\frac{3}{2}k_{\mathrm{B}}=2.0\ \mathrm{mK}\right)$, the transmission probabilities are $^1P_0^{(\mathrm{tun})}=0.66$, $^1P_1^{(\mathrm{tun})}=0.086$, and $^1P_2^{(\mathrm{tun})}=5.8\times10^{-4}$. Clearly, reflection is almost complete in the case of d-wave scattering (as E is much smaller than the barrier height), while transmission is significant for p-wave scattering. In the case of s-wave scattering, there is considerable reflection, although a centrifugal barrier is absent. Here, quantum reflection occurs due to the mismatch between the long asymptotic de Broglie wave and the rapidly oscillating wave in the region of small internuclear separation. We checked that the resulting partial-wave cross sections satisfy the quantum threshold behavior of Eq. (4).

To determine the dependence of the cross sections on the adapted short-range part of the potential, we have calculated the variation in the cross sections as a function of R_0 for various collision energies. If R_0 is close to the location of the potential curve minimum at $6.1a_0$, the variations are smallest (less than 0.2%). Furthermore, the difference between probabilities $^1P_\ell^{(\mathrm{tun})}$ and $^3P_\ell^{(\mathrm{tun})}$ at a given collision energy E is only a few percent, as potentials $^1\tilde{V}(R)$ and $^3\tilde{V}(R)$ differ very little in the region where elastic scattering takes place: $|^3\tilde{V}(R)-|^1\tilde{V}(R)|/|^1\tilde{V}(R)|<10^{-4}$ for $R>20a_0$.

It has been shown in calculations that the ionization cross sections for $^4He^*$ are enhanced if the s-wave scattering length ^5a associated with the quintet potential is near a singularity [15]. The s-wave scattering length describes elastic collisions in the low-temperature limit [37] and shows a singularity (goes through $\pm\infty$) whenever a bound state is removed from the potential [15]. From experiments, it has been determined that $^5a=7.6$ nm with an error of 0.6 nm [43]. The scattering length is sufficiently far from the singularity to neglect enhancement of the ionization cross sections. For $^3He^*$ atoms, the s-wave scattering length for $S=2$ is predicted to be $5.0<{}^5a<6.0$ nm [44]. This is also sufficiently small to neglect effects on the ionization cross sections.

D. Ionization rate coefficient

The ion production rate dN_{ion}/dt in a magneto-optically trapped atomic sample of $^3He^*$ or $^4He^*$ atoms can be expressed in terms of an ionization rate coefficient K (particle^{-1} cm^3/s),

$$\frac{dN_{\mathrm{ion}}(t)}{dt}=K\int\int\int n^2(\boldsymbol{r},t)d^3r. \tag{11}$$

The rate coefficient depends on the temperature T of the sample and can be written as [18]

$$K(T)=\int_0^\infty \sigma^{(\mathrm{ion})}(v_{\mathrm{r}})P_T^{(\mathrm{MB})}(v_{\mathrm{r}})v_{\mathrm{r}}dv_{\mathrm{r}}, \tag{12}$$

with

$$P_T^{(\mathrm{MB})}(v_{\mathrm{r}})=\sqrt{\frac{2}{\pi}}\frac{v_{\mathrm{r}}^2}{(k_{\mathrm{B}}T/\mu)^{3/2}}\exp\left(-\frac{v_{\mathrm{r}}^2}{2k_{\mathrm{B}}T/\mu}\right), \tag{13}$$

the Maxwell-Boltzmann distribution for the relative velocity in the atomic sample under study, with $\langle v_{\mathrm{r}}^2\rangle^{1/2}=(k_{\mathrm{B}}T/\mu)^{1/2}=(2k_{\mathrm{B}}T/m)^{1/2}$.

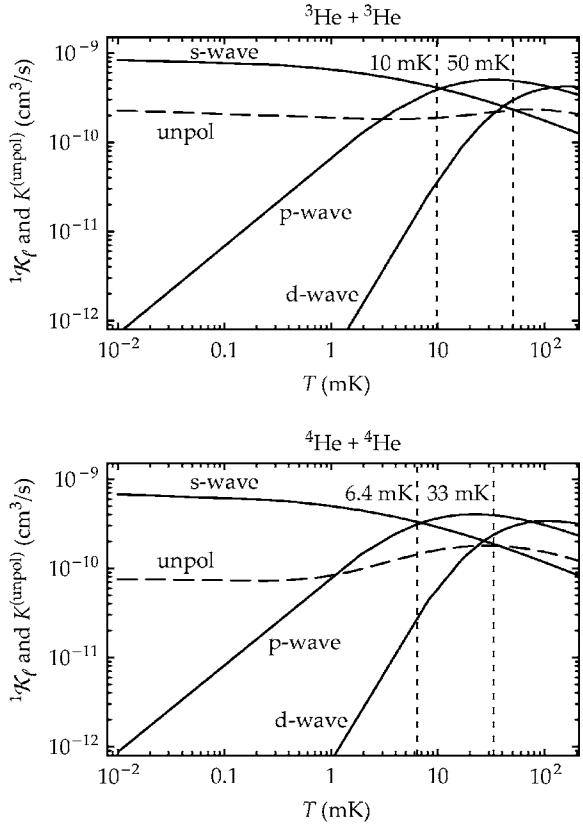

FIG. 3. Partial-wave ionization rate coefficients $^1\mathcal{K}_\ell$ and unpolarized rate coefficient $K^{(\mathrm{unpol})}$ for ^{3}He* and ^{4}He* ($^3\mathcal{K}_\ell$ coefficients are, within a percent, equal to corresponding $^1\mathcal{K}_\ell$ coefficients).

Correspondingly, we can define partial-wave ionization rate coefficients,

$$^{(2S+1)}\mathcal{K}_\ell(T) = \int_0^\infty {}^{(2S+1)}\sigma_\ell^{(\mathrm{ion})}(v_\mathrm{r}) P_T^{(\mathrm{MB})}(v_\mathrm{r}) v_\mathrm{r} dv_\mathrm{r}, \quad (14)$$

and the ionization rate coefficient associated with potential $^{(2S+1)}V(R)$,

$$^{(2S+1)}K(T) = \sum_\ell {}^{(2S+1)}\mathcal{K}_\ell(T). \quad (15)$$

Figure 3 shows plots of the rate coefficients (calculated with numerical integration) for a temperature range from 10 μK to 100 mK, for collisions of ^{3}He* or ^{4}He* atoms. The energy of the centrifugal barriers for $\ell=1$ and 2 is indicated by dashed vertical lines. For temperatures $T<5$ mK, the contribution of the d wave becomes very small and can be ignored if an accuracy of 5% is sufficient.

The quantum threshold behavior of the rate coefficients is given by

$$^{(2S+1)}\mathcal{K}_\ell \propto k^{2\ell} \quad \text{if } k \to 0. \quad (16)$$

In particular, we find $^{(2S+1)}\mathcal{K}_0 \to$ const if $k \to 0$, as the divergence of σ_0 is canceled by $v = \hbar k/\mu$. The differences between the two isotopes are less than 50%.

We have neglected the atomic hyperfine structure of the interatomic potentials for ^{3}He*. As it is four orders of magnitude smaller than the attractive interaction at short range, its effect on $^{(2S+1)}\sigma_\ell^{(\mathrm{ion})}$ and $^{(2S+1)}\mathcal{K}_\ell$ is negligible.

E. Symmetrization of scattering states

Although the interatomic interaction is almost identical in the case of ^{3}He* and ^{4}He*, giving rise to partial-wave contributions $^{(2S+1)}\sigma_\ell^{(\mathrm{ion})}$ and $^{(2S+1)}\mathcal{K}_\ell$ that are similar, the composition of the total ionization cross section or rate coefficient from these contributions is very different for the bosonic (^{4}He*) and fermionic isotope (^{3}He*). The symmetrization postulate requires that a scattering state describing a colliding pair of identical bosons has even symmetry under exchange of the atoms, while a state describing identical fermions has odd symmetry [45,46]. As a result, partial waves with improper symmetry do not contribute to the total cross section or rate coefficient, and are excluded from the summations in Eqs. (3) and (15).

1. Bosonic: ^{4}He* *Symmetric states*

The total electronic spin **S** and relative angular momentum ℓ of two colliding ^{4}He* atoms are, to good approximation, conserved separately [19,20], and S and ℓ can be considered good quantum numbers. Ignoring the radial part of the quantum states, a basis for atom pairs is given by

$$\{|(s_1)_A(s_2)_B, SM_S, \ell\, m_\ell\rangle\}. \quad (17)$$

For the moment, the atoms are assumed to be distinguishable and are labeled with A and B. The atoms carry spins $s_1=1$ and $s_2=1$, respectively, and the total electronic spin S is the result of the addition of s_1 and s_2. Quantum numbers M_S and m_ℓ are associated with the projection onto the internuclear axis of the total electronic spin and the relative angular momentum ℓ, respectively.

For a system of identical bosons, such as a pair of ^{4}He* atoms, physical states are symmetric under exchange of the two atoms. Such states are obtained by applying the symmetrizer $S=(1+P_{12})/\sqrt{2}$ to the basis vectors [36,47],

$$|s_1 s_2, SM_S, \ell\, m_\ell\rangle = \frac{1}{\sqrt{2}}[1+(-1)^{S+\ell}]|(s_1)_A(s_2)_B, SM_S, \ell\, m_\ell\rangle, \quad (18)$$

and normalizing the result if necessary. As the states differ from zero only if $S+\ell$ is even, we can conclude that it is not possible to construct states with the proper symmetry if $S=0$ or 2 and ℓ is odd, or if $S=1$ and ℓ is even. Consequently, the corresponding partial-wave ionization rate coefficients are excluded from the summation of Eq. (15) and we can write

$$^1K = \sum_{\ell\ \text{even}} {}^1\mathcal{K}_\ell, \quad (19)$$

$$^3K = \sum_{\ell\ \text{odd}} {}^3\mathcal{K}_\ell. \quad (20)$$

As total electronic spin is conserved, each long-range scattering state converts to a single short-range molecular state

associated with a potential of Fig. 1. Consequently, the strong suppression of ionization in the quintet potential results in a rate coefficient ${}^5K \approx 0$.

2. *Fermionic:* ^{3}He* *Antisymmetric states with hyperfine structure*

In a collision of two ^{3}He* atoms, the total atomic angular momentum $\mathbf{F}=\mathbf{f}_1+\mathbf{f}_2$ and the relative angular momentum of the two atoms ℓ are, to good approximation, conserved separately. Here, $\mathbf{f}_j=\mathbf{s}_j+\mathbf{i}_j$ $(j=1,2)$; the total angular momentum $\mathbf{f}_j$ of an atom is the sum of its electronic spin $\mathbf{s}_j$ and nuclear spin $\mathbf{i}_j$.

Ignoring the radial part of the quantum states and assuming for the moment that the colliding atoms are distinguishable, a basis for atom pairs is given by

$$\{|(s_1 i_1 f_1)_A (s_2 i_2 f_2)_B, F M_F, \ell\, m_\ell\rangle\}, \tag{21}$$

where atoms A and B have identical electronic spins $s_1=s_2=1$ and nuclear spins $i_1=i_2=\frac{1}{2}$, which add up to f_1 for atom A and f_2 for atom B. The latter two add up to the total atomic angular momentum F with projection onto the internuclear axis M_F. In magneto-optically trapped ^{3}He* samples, all atoms occupy the lower $f=\frac{3}{2}$ hyperfine level, so that $f_1=f_2=\frac{3}{2}$ and F can take values $0,1,2$, and 3. The quantum numbers ℓ and m_ℓ are the angular momenta associated with the relative motion of the two atoms and its projection onto the internuclear axis, respectively.

As the ^{3}He atom is a fermion, the physical states describing atom pairs are antisymmetric under exchange of the atoms. Applying the antisymmetrizer $\mathrm{A}=(1-\mathrm{P}_{12})/\sqrt{2}$ to the basis states [36,47], we obtain

$$\begin{aligned}&|s_1 i_1 f_1, s_2 i_2 f_2, F M_F, \ell\, m_\ell\rangle \\ &\quad = \frac{1}{\sqrt{2}}[1+(-1)^{\ell-F}]|(s_1 i_1 f_1)_A (s_2 i_2 f_2)_B, F M_F, \ell\, m_\ell\rangle.\end{aligned} \tag{22}$$

These states, which must be normalized if necessary, differ from zero only if $F-\ell$ is even. Consequently, only even (odd) partial waves contribute to collisions with even (odd) F, and the total ionization rate coefficient can be written

$$K(F) = \begin{cases} \sum_{\ell \text{ even}} \mathcal{K}_\ell(F) & \text{if } F = 0,2, \\ \sum_{\ell \text{ odd}} \mathcal{K}_\ell(F) & \text{if } F = 1,3. \end{cases} \tag{23}$$

To express the partial-wave rate coefficient $\mathcal{K}_\ell(F)$ in terms of the rate coefficients ${}^{(2S+1)}\mathcal{K}_\ell$ that are associated with singlet and triplet potentials, we consider the interaction between two colliding ^{3}He* atoms.

The collision process of two laser-cooled ^{3}He* atoms is controlled by the atomic hyperfine interaction [48] and the various interatomic interactions [38,40,41] that result in potentials ${}^{(2S+1)}V(R)$. As a result of the hyperfine interaction, S is not a good quantum number for large internuclear distances, where atom pairs are characterized by F. However, S is a good quantum number for $R \lesssim 30a_0$, where the molecular interaction dominates and Wigner's spin-conservation rule applies. The evolution of the quantum-mechanical state from long to short internuclear distance is well approximated by a diabatic transition, as the absolute change in the coupling between quasimolecular states, during one period of oscillation in the quasimolecular system, is much larger than the absolute energy difference between the scattering states [49,50]. Around $R=35a_0$, the molecular interaction, increasing exponentially with decreasing R [15], becomes larger than the atomic hyperfine interaction, while the relative velocity has increased to 4×10^{-5} a.u. due to the attractive Van der Waals potential. Consequently, the asymptotic scattering state of a colliding atom pair remains unchanged when the atoms reach small internuclear distance and the relation between rate coefficient $\mathcal{K}_\ell(F)$ and coefficients ${}^{(2S+1)}\mathcal{K}_\ell$ can be determined by expanding the corresponding scattering state onto the molecular states.

The expansion coefficients only depend on the angular part of the quantum states involved. For the molecular states, the angular part can be derived by applying the antisymmetrizer to the basis

$$\{|(s_1 i_1)_A (s_2 i_2)_B, S I, F M_F, \ell\, m_\ell\rangle\} \tag{24}$$

(and normalizing if necessary), where the atoms A and B are assumed distinguishable, I is the quantum number associated with the sum of the nuclear spins, $\mathbf{I}=\mathbf{i}_1+\mathbf{i}_2$, and S is the quantum number associated with the sum of the electronic spins, $\mathbf{S}=\mathbf{s}_1+\mathbf{s}_2$; the bases of Eqs. (21) and (24) are related through 9-j symbols [51]. The resulting physical states

$$\begin{aligned}|s_1 i_1, s_2 i_2, S I, F M_F, \ell\, m_\ell\rangle &= \frac{1}{\sqrt{2}}[1+(-1)^{\ell-S-I}] \\ &\quad \times |(s_1 i_1)_A (s_2 i_2)_B, S I, F M_F, \ell\, m_\ell\rangle\end{aligned} \tag{25}$$

are different from zero only if $\ell-S-I$ is even. The expansion of a scattering state onto the molecular states can be confined within the subspace defined by F and ℓ, as F and ℓ can be considered good quantum numbers,

$$\begin{aligned}|s_1 i_1 f_1, s_2 i_2 f_2, F M_F, \ell\, m_\ell\rangle &= \sum_{S,I} a_{SI}(F) \\ &\quad \times |s_1 i_1, s_2 i_2, S I, F M_F, \ell\, m_\ell\rangle.\end{aligned} \tag{26}$$

Table I presents the expansion coefficients $a_{SI}(F)$ for scattering states with $f_1=f_2=\frac{3}{2}$.

The partial wave rate coefficient $\mathcal{K}_\ell(F)$ associated with scattering state $|s_1 i_1 f_1, s_1 i_1 f_2, F M_F, \ell\, m_\ell\rangle$ can be written as a weighted sum of coefficients ${}^{(2S+1)}\mathcal{K}_\ell$ associated with molecular states $|s_1 i_1, s_1 i_1, S I, F M_F, \ell\, m_\ell\rangle$ with weights $|a_{SI}(F)|^2$,

$$\mathcal{K}_\ell(F) = \sum_{S,I} |a_{SI}(F)|^2 \times {}^{(2S+1)}\mathcal{K}_\ell. \tag{27}$$

It can be seen in Table I that, in the case of $F=0$, only singlet and triplet states are involved, so that

TABLE I. Expansion coefficients $a_{SI}(F)=\langle s_1 i_1, s_2 i_2, SI, FM_F, \ell m_\ell | s_1 i_1 f_1, s_2 i_2 f_2, FM_F, \ell m_\ell\rangle$. Scattering state $|s_1 i_1 f_1, s_2 i_2 f_2, FM_F, \ell m_\ell\rangle$ is indicated by its values of F, while molecular state $|s_1 i_1, s_2 i_2, SI, FM_F, \ell m_\ell\rangle$ is denoted in the Hund's case (a) notation $^{2S+1}\Sigma^+_{g/u}(I)$.

F	$^1\Sigma^+_g$ $(I=0)$	$^1\Sigma^+_g$ $(I=1)$	$^3\Sigma^+_u$ $(I=0)$	$^3\Sigma^+_u$ $(I=1)$	$^5\Sigma^+_g$ $(I=0)$	$^5\Sigma^+_g$ $(I=1)$
0	$\sqrt{2/3}$			$-\sqrt{1/3}$		
1		$\sqrt{10/27}$	$\sqrt{5/9}$			$-\sqrt{2/27}$
2				$\sqrt{2/3}$	$\sqrt{1/3}$	
3						1

$$\mathcal{K}_\ell(0) = \tfrac{2}{3}(^1\mathcal{K}_\ell) + \tfrac{1}{3}(^3\mathcal{K}_\ell). \tag{28}$$

For the $F=1$ and 2 states, the diabatic transition transforms the scattering states into a superposition of ionizing and nonionizing molecular states. The contribution to the ionization rate coefficient from quintet states can be neglected, so that

$$\mathcal{K}_\ell(1) = \tfrac{10}{27}(^1\mathcal{K}_\ell) + \tfrac{5}{9}(^3\mathcal{K}_\ell), \tag{29}$$

$$\mathcal{K}_\ell(2) = \tfrac{2}{3}(^1\mathcal{K}_\ell). \tag{30}$$

Finally, in the case of $F=3$, the partial rate coefficient $\mathcal{K}_\ell(3)$ is negligible, as only quintet states are involved.

F. Ionization rate coefficient for trapped samples

In a laser-cooled sample of He^* atoms, collisions occur for all values of the total atomic angular momentum $F=0,1,2,3$ in the case of $^3He^*$, and $S=0,1,2$ in the case of $^4He^*$. The contribution of each collision channel depends on the distribution P_m of magnetic substates in the sample, where m is the azimuthal quantum number of the atom, which can take on values $m_f=-\frac{3}{2},-\frac{1}{2},\frac{1}{2},\frac{3}{2}$ in the case of $^3He^*$ and $m_s=-1,0,1$ in the case of $^4He^*$. Using the density operator [36]

$$\rho(\boldsymbol{r}) = \sum_m \sum_{n\le m} P_m(\boldsymbol{r}) P_n(\boldsymbol{r}) |m,n\rangle\langle m,n| \tag{31}$$

to describe a statistical mixture of (properly symmetrized) magnetic substate pairs $|m,n\rangle$, with m and n azimuthal quantum numbers, the ionization rate coefficient for the mixture [cf. Eq. (11)] can be written as

$$K = \frac{1}{N}\int\int\int \left(\sum_{\ell\ \text{even}} (^1b_{\text{even}}\,^1\mathcal{K}_\ell + {}^3b_{\text{even}}\,^3\mathcal{K}_\ell) + \sum_{\ell\ \text{odd}} (^1b_{\text{odd}}\,^1\mathcal{K}_\ell + {}^3b_{\text{odd}}\,^3\mathcal{K}_\ell) \right) n(\boldsymbol{r}) d^3r, \tag{32}$$

where N is the number of trapped atoms, $n(\boldsymbol{r})$ is the density distribution in the sample, and $^{(2S+1)}b_{\text{even/odd}}$ is the sum of the expectation values of the density operator for all ionizing molecular states with total spin S and even (odd) parity. Explicit expressions for the coefficients are given in Table II. As the coefficients can be interpreted as projections of the statistical mixture onto subspaces of ionizing states, Eq. (32) implies the assumption that scattering states transform diabatically to a superposition of molecular states, when atoms move from large to small internuclear distance.

The unpolarized ionization rate coefficients $K^{(\text{unpol})}$, i.e., the rate coefficient for a laser-cooled sample of He^* atoms where the magnetic substates of the atoms are uniformly populated, is obtained by setting $P_{-1}=P_0=P_1=\frac{1}{3}$ for $^4He^*$ or $P_{-3/2}=P_{-1/2}=P_{1/2}=P_{3/2}=\frac{1}{4}$ for $^3He^*$. For samples with a temperature around 1 mK, only s and p waves have to be taken into account. For unpolarized $^4He^*$ samples, we obtain

$$K^{(\text{unpol})}_{^4\text{He}} \approx \tfrac{1}{9}[(^1\mathcal{K}_0) + 3(^3\mathcal{K}_1)], \tag{33}$$

where $^1\mathcal{K}_0$ and $^3\mathcal{K}_1$ are the partial-wave ionization rate coefficients for $^4He^*$, calculated in Sec. II C. In the case of an unpolarized sample of $^3He^*$ atoms in the lower $f=\frac{3}{2}$ hyperfine level, the rate coefficient is given by

TABLE II. Coefficients $^{(2S+1)}b_{\text{even/odd}}$ from Eq. (32). The coefficients are the sums of the expectation values of the density operator for all ionizing molecular states of given S and given parity.

	$^3He^*$	$^4He^*$
$^1b_{\text{even}}$	$(1/3)(P_{-3/2}P_{3/2}+P_{-1/2}P_{1/2})$	$(1/3)(2P_{-1}P_1+P_0^2)$
$^3b_{\text{even}}$	$(2/3)(P_{-3/2}P_{-1/2}+P_{-3/2}P_{1/2}+P_{-1/2}P_{3/2}+P_{1/2}P_{3/2})$ $+(1/2)(P_{-3/2}P_{3/2}+P_{-1/2}P_{1/2})$	0
$^1b_{\text{odd}}$	$(2/9)(P_{-3/2}P_{1/2}+P_{-1/2}P_{3/2})+(4/27)(P_{-1/2}P_{-1/2}$ $+P_{1/2}P_{1/2})+(1/3)P_{-3/2}P_{3/2}+(1/27)P_{-1/2}P_{1/2}$	0
$^3b_{\text{odd}}$	$(1/3)(P_{-3/2}P_{1/2}+P_{-1/2}P_{3/2})+(2/9)(P_{-1/2}P_{-1/2}$ $+P_{1/2}P_{1/2})+(1/2)P_{-3/2}P_{3/2}+(1/18)P_{-1/2}P_{1/2}$	$P_{-1}P_0+P_{-1}P_1+P_0P_1$

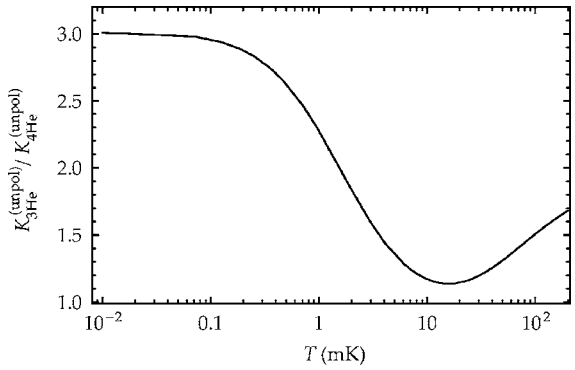

FIG. 4. Ratio of unpolarized ionization rate coefficients $K_{^3\mathrm{He}}^{(\mathrm{unpol})}/K_{^4\mathrm{He}}^{(\mathrm{unpol})}$, including partial-wave contributions up to $\ell=2$.

$$K_{^3\mathrm{He}}^{(\mathrm{unpol})} \approx \tfrac{1}{16}\left[\tfrac{11}{3}({}^1\mathcal{K}_0) + \tfrac{2}{3}({}^3\mathcal{K}_0) + \tfrac{10}{9}({}^1\mathcal{K}_1) + \tfrac{5}{3}({}^3\mathcal{K}_1)\right], \tag{34}$$

where ${}^1\mathcal{K}_0$, ${}^3\mathcal{K}_0$, ${}^1\mathcal{K}_1$, and ${}^3\mathcal{K}_1$ are the partial-wave ionization rate coefficients for ^{3}He*. For both isotopes, the coefficients are shown in Fig. 3 for temperatures between 10 μK and 100 mK. It can be seen in Fig. 4, where the ratio of the unpolarized rate coefficients for the two isotopes is displayed, that unpolarized ^{3}He* atoms have a larger rate coefficient than unpolarized ^{4}He* atoms for temperatures between 10 μK and 100 mK.

In Table III, we compare the results of the theoretical model presented here to results of other theoretical work [8,11,15]. We see that our results agree well with the results of the detailed close-coupling theory of [15] and the simpler calculation of [8], but that there is a large discrepancy with the results of Kumakura and Morita [11]. This is not surprising, since their model does not account for quantum reflection for *s*-wave scattering. As we have shown in Sec. II C, quantum reflection is significant and we estimate that the omission of this effect leads to rate coefficients that are too large by factor of about 2. Moreover, Kumakura and Morita assume that the evolution of the scattering states during the collision of two ^{3}He* atoms can be approximated by an adiabatic transition and accordingly apply the noncrossing rule [52] to derive the number of ionization channels for each partial-wave ionization rate coefficient. As shown in Sec. II E, the system is well approximated by a diabatic transition and we estimate that the assumption of an adiabatic transition leads to an unpolarized rate coefficient that is 50% too large. This explains the difference between our results and those of Ref. [11]. As a final remark we note that the observed differences between our work and those of Refs. [8,15] may be due to theoretical uncertainties in the molecular potentials and in the form of the ionization widths used in the calculations. This leads to theoretical uncertainties of $\approx$40%, as discussed in Ref. [15].

TABLE III. Calculated values of $K^{(\mathrm{unpol})}$ and comparison between various theoretical results. Theoretical results from Ref. [15] are extracted from Fig. 8 of that paper.

	Ref.	T (mK)	$K^{(\mathrm{unpol})}$ (cm^3/s)	This work
^{4}He*	[15]	0.001	9.9×10^{-11}	7.7×10^{-11}
	[11]	0.5	2.2×10^{-10}	7.5×10^{-11}
	[15]	0.5	8.6×10^{-11}	7.5×10^{-11}
	[8]	1	7.3×10^{-11}	8.3×10^{-11}
	[15]	1	8.9×10^{-11}	8.3×10^{-11}
		2		9.9×10^{-11}
^{3}He*	[11]	0.5	1.0×10^{-9}	2.0×10^{-10}
		2		1.8×10^{-10}

III. MEASUREMENT OF IONIZING COLLISIONS IN A MAGNETO-OPTICAL TRAP

The experimental investigation of ionizing collisions is performed in a setup that can be used to confine large numbers ($\gtrsim10^8$) of atoms in a MOT. As the setup has been described previously [5], only a brief outline is presented here. The MOT is loaded from a collimated and Zeeman-slowed atomic beam, produced by a liquid-nitrogen-cooled dc-discharge source. The beam source can be operated with pure ^{3}He* or pure ^{4}He* gas. In the case of ^{3}He*, the gas is recycled and purified using liquid-nitrogen-cooled molecular sieves.

The laser light that is used for collimation, Zeeman slowing, and magneto-optical trapping has a wavelength of 1083 nm and is near resonant with the $2\,{}^3\mathrm{S}_1\left(f=\frac{3}{2}\right) \rightarrow 2\,{}^3\mathrm{P}_2\left(f=\frac{5}{2}\right)$ optical transition in the case of ^{3}He*, and the $2\,{}^3\mathrm{S}_1 \rightarrow 2\,{}^3\mathrm{P}_2$ transition in the case of ^{4}He*. For both transitions, the natural linewidth $\Gamma/2\pi=1.62$ MHz and the saturation intensity $I_{\mathrm{sat}}=0.167$ mW/cm^2 (cycling transition). The light is generated by an ytterbium-doped fiber laser, which is frequency stabilized to the laser-cooling transition using saturated absorption spectroscopy in an rf-discharge cell. Acousto-optic modulators (AOMs) are used to generate the slowing and trapping frequencies, which are detuned by -500 and -40 MHz, respectively. The slowing beam is focused onto the atomic beam source, while the trapping light is split up into six independent Gaussian beams with rms diameter of 27 mm and a total peak intensity $I_{\mathrm{peak}}=59$ mW/cm^2 ($I_{\mathrm{peak}}/I_{\mathrm{sat}}\approx353$). The magnetic quadrupole field of the MOT is generated by two anti-Helmholtz coils and has an axial field gradient $\partial B/\partial z=0.28$ T/m.

For the investigation of ionizing collisions, the trapped He* samples are studied with an absorption imaging system and two microchannel plate detectors [50]. The absorption imaging system consists of a charge-coupled device (CCD) camera, a narrowband commercial diode laser at 1083 nm (TOPTICA, model DL100), and an AOM. The laser and AOM are used to generate low-intensity ($I\lesssim0.05I_{\mathrm{sat}}$) probe light pulses with a duration of 100 μs, while the CCD camera (mounted behind a magnifier lens) records absorption images of the sample with a magnification of 0.17. The images are used to determine the (Gaussian) density distribution of the atoms in the trap [50],

$$n(x,y,z,t) = n_0(t)\exp\left(-\frac{x^2}{2\sigma_\rho^2}-\frac{y^2}{2\sigma_\rho^2}-\frac{z^2}{2\sigma_z^2}\right), \tag{35}$$

with $n_0(t)$ the (time-dependent) density in the center ($x=y=z=0$) of the sample, and σ_ρ and σ_z the rms radii of the

distribution; the number of trapped atoms $N=\int\int\int n(\boldsymbol{r})d^3r = (2\pi)^{3/2}\sigma_\rho^2\sigma_z n_0$.

The MCP detectors allow for the independent monitoring of ions and He^* atoms that escape the trap. With an exposed negative high voltage on its front plate, one MCP detector attracts all ions produced in the trapped sample. The other MCP is mounted behind a grounded grid and detects only the He^* atoms that exit the trap in its direction. This shielded MCP detector is used to determine the temperature T of the trapped samples through time-of-flight measurements. The unshielded MCP detector measures the instantaneous ionization rate in the trapped sample and is used to determine trap loss and ionization rates in the sample.

A. Trap loss and ionization in magneto-optical trap

For magneto-optically trapped He^* samples, the time evolution of the number of trapped atoms N can be described by the phenomenological equation [7,13]

$$\frac{dN(t)}{dt} = L - \alpha N(t) - \beta \int\int\int n^2(\boldsymbol{r},t)d^3r. \tag{36}$$

Writing down this differential equation, we assume that $N(t)$ is controlled by three simultaneously occurring processes, corresponding to the three terms on the right-hand side of the equation. The first term is a constant loading rate L, representing the capture of atoms from the decelerated atomic beam into the MOT. The second and third terms are the linear and quadratic trap loss rates, respectively. The loss processes are defined in terms of the local atomic density of the sample $n(\boldsymbol{r},t)$ (with $L=0$) by

$$\frac{dn(\boldsymbol{r},t)}{dt} = -\alpha n(\boldsymbol{r},t) - \beta n^2(\boldsymbol{r},t). \tag{37}$$

The nomenclature of the loss rate terms refers to their proportionality to density $n(\boldsymbol{r},t)$ and density squared $n^2(\boldsymbol{r},t)$. Analogously, the proportionality constants α and β are referred to as the linear and quadratic loss rate coefficients, respectively.

For He^* samples in a 1083 nm MOT, only collisional loss mechanisms give rise to significant trap loss. Quadratic trap loss is determined by collisions between trapped He^* atoms, while linear trap loss results from collisions with particles traversing the trapping volume, such as background gas particles and helium atoms from the atomic beam. Loss rates in $^4He^*$ samples can be estimated using cross section data reported in the literature [22,53]. Table IV presents an overview of trap loss mechanisms in $^4He^*$ samples; cross-section data are combined with the atomic density in the sample, the background gas density, or the atomic beam flux to determine the estimates.

The trap loss mechanisms can be subdivided into ionizing mechanisms and mechanisms where atoms are lost without the formation of ions. Linear trap loss is dominated by a nonionizing loss mechanism. As the beam of metastable atoms is not separated from the beam of ground-state atoms (contrary to other work [10,13,14,21]), collisions of ground-state ^4He atoms from the atomic beam with trapped atoms (collision energy $E_r \approx 4.9$ meV) give rise to a trap loss rate of about 2 s^{-1}. Ionizing mechanisms hardly contribute: collisions with slowed ($E_r \approx 0.0064$ meV) and nonslowed $^4He^*$ atoms ($E_r \approx 6.5$ meV) from the atomic beam, and collisions with background molecules (presumably H_2O, H_2, N_2, and O_2) result in a loss rate of about 1×10^{-2} s^{-1}.

Quadratic trap loss is dominated by ionization mechanisms. In the presence of trapping light, light-assisted ionizing collisions between trapped $^4He^*$ atoms give rise to an ionization rate of 4 s^{-1}. In the absence of trapping light, ionizing collisions yield a rate of 0.1 s^{-1}. As two atoms are lost for every ion that is formed, the corresponding trap loss rates are 8 and 0.2 s^{-1}, respectively. The escape of fast $^4He^*$ atoms from the trap, through fine-structure-changing collisions or radiative escape, constitutes a nonionizing quadratic loss mechanism in the presence of trapping light, which can be neglected [54,55].

The ionization rate associated with the linear and quadratic ionization mechanisms can be written as

$$\frac{dN_{\mathrm{ion}}(t)}{dt} = \epsilon_a\alpha N(t) + \frac{\epsilon_b\beta}{2}\int\int\int n^2(\boldsymbol{r},t)d^3r, \tag{38}$$

where ϵ_a and ϵ_b are the weights of ionization mechanisms in linear and quadratic trap loss, respectively. The quadratic ionization rate is half of the ionizing quadratic trap loss rate, as a single ion is formed for every pair of colliding He^* atoms that is lost from the trap. As the linear ionization rate is small compared to the quadratic ionization rate, in both the presence and absence of trapping light, and quadratic trap loss is almost completely determined by ionization mechanisms, we can set, to good approximation, $\epsilon_a=0$ and $\epsilon_b=1$, so that

$$\frac{dN_{\mathrm{ion}}(t)}{dt} \approx \frac{\beta}{2}\int\int\int n^2(\boldsymbol{r},t)d^3r. \tag{39}$$

For samples of $^3He^*$ atoms, trap loss and ionization are determined by the same loss mechanisms. As collision studies are rare for $^3He^*$ atoms [22,53], we cannot derive accurate estimates of trap loss and ionization rates in this case. However, cross sections are not expected to show a large isotopic dependence (less than a factor of 2), so we conclude that Eq. (39) also applies to $^3He^*$ samples. It should be noted in this respect that hyperfine-changing collisions are forbidden by energy conservation. Trapped $^3He^*$ atoms are in the lower $f=\frac{3}{2}$ hyperfine level, so that hyperfine-changing collisions require an energy larger than the hyperfine splitting $E_{\mathrm{hf}}=28$ μeV, which corresponds to a temperature $E_{\mathrm{hf}}/\frac{3}{2}k_{\mathrm{B}} = 0.2$ K.

B. Ionization rates for light-assisted collisions

To determine the ionization rate coefficient for light-assisted collisions, $\epsilon_b\beta/2 \approx \beta/2$, we have performed a trap loss experiment, where the loading of atoms to the MOT is abruptly stopped and the decaying ionization rate in the sample is monitored with the unshielded MCP detector. For Gaussian samples, described by Eq. (35), the ionization rate can be written as

TABLE IV. Trap loss rate dN/dt and ionization rate dN_{ion}/dt associated with collisional loss mechanisms in magneto-optically trapped samples of $^4He^*$ atoms. Rates are calculated for collisions of trapped $^4He^*$ atoms with ground-state ($1\,^1S$) ^4He atoms and metastable ($2\,^3S$) $^4He^*$ atoms from the atomic beam, for collisions with ground-state ^4He atoms and several molecules from the thermal background gas, and for collisions between trapped $^4He^*$ atoms from the sample, in both the presence and absence of trapping light (with a wavelength of 1083 nm). For each collisional mechanism, the collision energy E_r is given, as well as total cross section $\sigma^{(\mathrm{tot})}$ or ionization cross section $\sigma^{(\mathrm{ion})}$. Furthermore, beam flux F, background gas density $\tilde{n}$, or central density n_0 of the sample are given. For collisions with $^4He^*$ atoms from the beam, we distinguish between slowed ($E_r=0.0064$ meV) and nonslowed ($E_r=6.5$ meV) atoms [50]. The cross sections are taken from various references; in references where an ionization rate coefficient K is given the corresponding cross section is calculated as $\sigma^{(\mathrm{ion})}=K/\bar{v}_r$, where $\bar{v}_r=(8k_BT/\pi\mu)^{1/2}$ is the mean relative velocity for collisions of particles with mass m_1 and m_2 in a gas with temperature T, with reduced mass $\mu=m_1m_2/(m_1+m_2)$.

Collision partner	Originating from	E_r (meV)	$\sigma^{(\mathrm{tot})}$ (10^{-16} cm^2)	$\sigma^{(\mathrm{ion})}$ (10^{-16} cm^2)	F (cm^{-2} s^{-1})	$\tilde{n}$ (cm^{-3})	n_0 (cm^{-3})	dN_{ion}/dt (s^{-1})	dN/dt (s^{-1})
^4He	beam	4.9	200[a]		$\sim10^{14}$		0	~2[b]	
$^4He^*$	beam	6.5		181[c]	4×10^{11}			7×10^{-3}[b]	1×10^{-2}[d]
$^4He^*$	beam	0.0064		1160[e]	8×10^{9}			9×10^{-4}[b]	2×10^{-3}[d]
^4He	background	16.5	140[f]			1×10^{7}		0	0.02[g]
H_2	background	22		0.1[h]		$<1.2\times10^{6}$		$<2\times10^{-4}$[g]	$<4\times10^{-4}$[d]
H_2O	background	6.0		131[i]		$<1.2\times10^{6}$		$<9\times10^{-4}$[g]	$<2\times10^{-3}$[d]
O_2	background	4.7		8[j]		$<1.2\times10^{6}$		$<4\times10^{-5}$[g]	$<8\times10^{-5}$[d]
N_2	background	4.1		2[k]		$<1.2\times10^{6}$		$<1\times10^{-5}$[g]	$<2\times10^{-5}$[d]
$^4He^*$	sample	0.00001		4×10^{3}[l]			4×10^{9}	0.1[m]	0.2[d]
$^4He^*$+light	sample	0.00001		16×10^{4}[l]			4×10^{9}	4[m]	8[d]

[a] Vrinceanu *et al.* [56].
[b] For collisions with atoms from the beam, rates are σF.
[c] For collision energies $0.1<E_r<100$ meV, $\sigma^{(\mathrm{ion})}$ satisfies the (semiclassical) energy dependence $\sigma^{(\mathrm{ion})}=\sigma_1(E_1/E_r)^{\alpha}$, with $E_1=1$ meV, $\sigma_1=318\times10^{-16}$ cm^2, and $\alpha=0.3$ [38].
[d] As two atoms are lost from the trap for each ion that is formed, $dN/dt=2(dN_{\mathrm{ion}}/dt)$.
[e] Venturi *et al.* [17].
[f] Mastwijk [57] and Rothe *et al.* [58].
[g] For collisions with background gas particles, rates are $\sigma\bar{v}_r\tilde{n}$,where $\bar{v}_r=(2E_r/\mu)^{1/2}$ is the mean relative velocity for collisions of particles with mass m_1 and m_2, with $\mu=m_1m_2/(m_1+m_2)$ their reduced mass.
[h] Martin *et al.* [59].
[i] Mastwijk [57]; the large cross section results from a large attractive force between $^4He^*$ and H_2O, a consequence of the permanent dipole moment of the H_2O molecule.
[j] Parr *et al.* [60].
[k] Yamazaki *et al.* [61].
[l] Tol *et al.* [10]; the cross section for light-assisted collisions is exceptionally large due to the optical excitation of the colliding atom pair to long-range dipole-dipole potentials [3].
[m] For samples with a Gaussian density distribution, as given by Eq. (35), quadratic ionization rate $dN_{\mathrm{ion}}/dt=(\sigma^{(\mathrm{ion})}\bar{v}_r/N)\int\int\int n^2(\boldsymbol{r})d^3r=\sigma^{(\mathrm{ion})}\bar{v}_rn_0/2\sqrt{2}$.

$$\frac{dN_{\mathrm{ion}}(t)}{dt}=V\frac{\beta}{4\sqrt{2}}n_0^2(t), \tag{40}$$

where the effective volume $V=(2\pi)^{3/2}\sigma_\rho^2\sigma_z$, such that central density $n_0(t)=N(t)/V$. The current signal from the MCP detector is proportional to the ionization rate and is converted to a voltage signal that is given by

$$\varphi(t)=eR_{\mathrm{eff}}\frac{\beta}{4\sqrt{2}}n_0^2(t), \tag{41}$$

where e is the electron charge and R_{eff} is an effective resistance.

Substitution of Eq. (35) into Eq. (36) shows that the central density satisfies the differential equation

$$\frac{dn_0(t)}{dt}=\frac{L}{V}-\alpha n_0(t)-\frac{\beta}{2\sqrt{2}}n_0^2(t). \tag{42}$$

If the loading of atoms to the MOT is abruptly stopped, the density decays as [2]

$$n_0(t)=\frac{n_0(0)}{\left(1+\frac{\beta n_0(0)}{2\sqrt{2}\alpha}\right)\exp(\alpha t)-\frac{\beta n_0(0)}{2\sqrt{2}\alpha}}. \tag{43}$$

Substitution of Eq. (43) into Eq. (41) gives an expression for the decaying ionization signal. The loss rates α and $\beta n_0(0)$ determine the exact shape of the decay and are derived from the measured traces by means of curve fitting.

We have performed trap loss measurements on $^3He^*$ and $^4He^*$ samples. The loading of atoms into the MOT is stopped

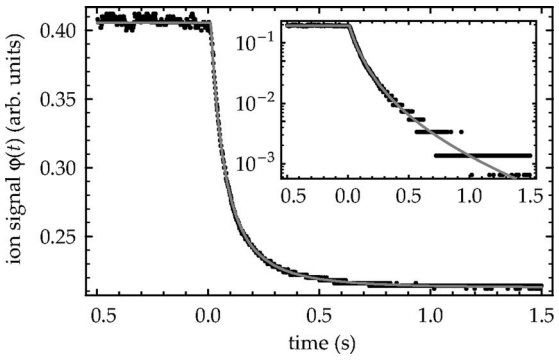

FIG. 5. Ionization signal for a trap loss measurement on a ^{3}He* sample. At $t=0$, the input of atoms to the MOT is stopped abruptly. The rapid decay of the ionization signal (black dots) is nonexponential, as can be seen in the inset. Fitting the signal to our model (gray line) yields trap loss rates $\beta n_0(0)=20$ s^{-1} and $\alpha=0.7$ s^{-1}.

by blocking the Zeeman-slowing light with the AOM used for frequency detuning the slowing light from the atomic transition. Decay traces are averaged four times using a digital oscilloscope. It has been verified that the variations in the central density are small enough that an averaged decay curve allows an accurate determination of loss rates α and $\beta n_0(0)$. An example of an averaged decay trace and the corresponding fit are displayed in Fig. 5. The central density in the samples $n_0(0)$ is derived from absorption imaging. The resulting rate coefficients α and β are presented in Table V.

The linear loss rate coefficients are close to 1 s^{-1} for both isotopes. Assuming that the loss rate stems from collisions with ground-state atoms from the atomic beam, we can determine the intensity of the beam of ground-state atoms. Using the total cross section $\sigma=200\times10^{-16}$ cm^2 [56] for collisions between trapped ^{4}He* atoms and ground-state ^{4}He atoms from the atomic beam, the distance between source and trapped sample of 370 cm, and loss rate coefficient $\alpha=0.6$ s^{-1}, we derive an intensity of 4×10^{18} s^{-1} sr^{-1}. As the intensity of ^{4}He* atoms is 4×10^{14} s^{-1} sr^{-1} [50], the fraction of ^{4}He* atoms in the beam is 10^{-4}.

The quadratic loss rate coefficient for ^{3}He* is almost twice as large as the loss rate coefficient for ^{4}He*. It has been pointed out that this isotopic difference stems from a difference in the relative number of ionization channels, opened up by the lowering of centrifugal barriers by the long-range, resonant dipole-dipole interaction [11]. Quantum-statistical symmetry requirements play a role in these collisions, but the effects are washed out as the number of participating partial waves is much larger than 1. The loss rate coefficient for ^{4}He* is in good agreement with other work [10].

TABLE V. Characteristic parameters of the magneto-optically trapped He* samples and extracted loss rate coefficients. Experimental errors correspond to one standard deviation.

	^{3}He*	^{4}He*
T (mK)	2.0(3)	1.9(1)
N	$2.6(9)\times10^8$	$3.7(5)\times10^8$
n_0 (cm^{-3})	$3.0(5)\times10^9$	$4.4(4)\times10^9$
α (s^{-1})	0.8(2)	0.6(3)
β (cm^3/s)	$5.5(8)\times10^{-9}$	$3.3(7)\times10^{-9}$
K (cm^3/s)	$1.8(3)\times10^{-10}$	$8(2)\times10^{-11}$
$K^{(\mathrm{unpol})}$ (cm^3/s)	$1.9(3)\times10^{-10}$	$10(2)\times10^{-11}$

C. Ionization in the absence of trapping light

Collisions where ionization is not preceded by absorption of trapping light contribute little to the ionization rate in magneto-optically trapped He* samples. However, the corresponding ionization rate coefficients can be determined from a comparative measurement of the ionization rate in the presence and absence of trapping light [7]. In this measurement, the trapping and slowing light are blocked for a short time interval of 100 μs with the AOMs used for the detuning of the laser frequencies from the atomic transition. With the trapping light present, the observed ionization signal

$$\varphi_{\mathrm{on}}(t) = eR_{\mathrm{eff}}\frac{\beta}{4\sqrt{2}}n_0^2(0) + \varphi_{\mathrm{bgr}} \tag{44}$$

is dominated by light-assisted collisions and is relatively large. If the trapping light is absent, collisions of ^{3}He* or ^{4}He* atoms occur without optical excitation; the corresponding ionization rate is much smaller and can be written as

$$\varphi_{\mathrm{off}}(t) = eR_{\mathrm{eff}}\frac{K}{2\sqrt{2}}n_0^2(0) + \varphi_{\mathrm{bgr}}, \tag{45}$$

with K the ionization rate coefficient in the absence of trapping light. Combing Eqs. (44) and (45), the rate coefficient can be written as

$$K = \frac{\beta}{2}\frac{\varphi_{\mathrm{off}} - \varphi_{\mathrm{bgr}}}{\varphi_{\mathrm{on}} - \varphi_{\mathrm{bgr}}}. \tag{46}$$

Clearly, K can be derived from a measurement of the ionization rate coefficient for light-assisted collisions, $\beta/2$, and signals φ_{on}, φ_{off}, and φ_{bgr}.

In the experiment, the trapping and slowing light are blocked every 200 ms, and the ionization signal is averaged 256 times with a digital oscilloscope. Examples of averaged ionization signals are displayed in Fig. 6. The measurement is repeated with the atomic beam blocked to obtain the background ionization signal φ_{bgr}, which includes an offset originating from the MCP signal amplifier. To obtain accurate values of $(\varphi_{\mathrm{on}}-\varphi_{\mathrm{bgr}})$ and $(\varphi_{\mathrm{off}}-\varphi_{\mathrm{bgr}})$, the average of the signals is determined over 40 μs time intervals, as indicated in Fig. 6.

Although the atoms are not confined if the trapping light is absent, the expansion of the trapped He* sample during 100 μs is insignificant and can be neglected. It is checked that the trapped sample remains unaffected if the light is blocked repeatedly, running the experiment with a duty cycle of 200 ms. The resulting ionization rate coefficients are presented in Table V. The coefficients are close to but do not agree within the error bars with other experimental results [8,10,11,21], which suffer from mutual inconsistency themselves, as has been pointed out [15].

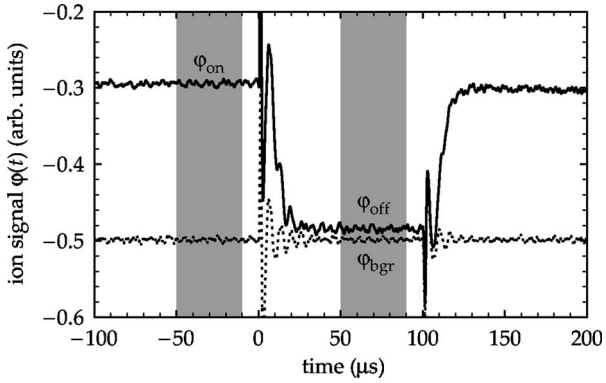

FIG. 6. Ionization rates in the presence and absence of trapping (and slowing) light. The signals are averaged over 40 μs time intervals indicated by the shaded areas to obtain $(\varphi_{on}-\varphi_{bgr})$ and $(\varphi_{off}-\varphi_{bgr})$.

D. Comparison between experiment and theory

To confront the theoretical model of Sec. II with the measurements of Secs. III B and III C, we compare the theoretical expression for K, Eq. (32), with the $T=2$ mK experimental values of Table V. As optical pumping processes cause the magnetic substate distribution to deviate from a uniform distribution (with the stretched substates slightly overpopulated), we need to determine the magnetic substate distribution $P_m(\boldsymbol{r})$ in the trapped samples to calculate a value for K that can be compared to experiment.

The distribution $P_m(\boldsymbol{r})$ is obtained as the steady-state solution of a rate equation model, which describes the optical pumping in the MOT [21]. Starting from the intensity and detuning of the trapping light, and an expression for the quadrupole magnetic field, rate equations are formulated and subsequently solved to obtain the steady-state substate population in the sample. In these calculations we take into account that the intensities of the trapping beams are not balanced and that (consequently) the trapped sample is not exactly centered on the zero point of the magnetic field.

At a temperature $T=2$ mK, the resulting theoretical ionization rate coefficients

$$K_{^3\mathrm{He}} = 1.7 \times 10^{-10}\ \mathrm{cm}^3/\mathrm{s}, \tag{47}$$

$$K_{^4\mathrm{He}} = 8.0 \times 10^{-11}\ \mathrm{cm}^3/\mathrm{s}, \tag{48}$$

agree very well with the experimental values of Table V. At this low temperature only s and p waves have to be taken into account as higher-order waves contribute less than a few percent. The samples are partially polarized, so that quadratic ionization rates are smaller than they would be in unpolarized samples. Because of the different substate structure ($s=1$ compared to $f=3/2$) and different quantum-statistical symmetry, the corrections for the two isotopes differ, $K_{^4\mathrm{He}}/K_{^4\mathrm{He}}^{(\mathrm{unpol})}=0.81$ and $K_{^3\mathrm{He}}/K_{^3\mathrm{He}}^{(\mathrm{unpol})}=0.93$. For direct comparison with the theoretical results of Table III $K^{(\mathrm{unpol})}$ for ^{3}He* and ^{4}He* have been included in Table V as well.

IV. DISCUSSION AND CONCLUSIONS

The theoretical model presented in Sec. II shows good agreement with other theoretical work and with the experimental results reported in Sec. III. The agreement between the various results has to be considered partly coincidental in view of the theoretical uncertainties in the potentials, as already mentioned in Sec. II F. Anyway, this shows that cold ionizing collisions of He* atoms can be understood as single-channel processes that are determined by Wigner's spin-conservation rule, quantum threshold behavior, and the symmetrization postulate. Using the model, the difference between the ionization rate coefficients for ^{3}He* and ^{4}He* can be interpreted as an effect of the different quantum-statistical symmetry of the two isotopes and the presence of a nuclear spin in the case of ^{3}He*; these differences do not depend on uncertainties related to the potential as the same potentials (with mass scaling) were used in the ^{4}He* and ^{3}He* cases. As the model is relatively simple, it is complementary to the more complete (and precise) close-coupling theory that has been developed for ^{4}He* collisions [15–17]. Another single-channel model that was published recently [11] was shown to be based on erroneous assumptions.

The experimental values of Sec. III do not agree with other (mutually inconsistent) experimental results [8,10,11,21]. The discrepancy between the experimental values is difficult to interpret, as the experimental determination of the ionization rate coefficient is the result of an extensive analysis, including the determination of the density distribution and temperature of the trapped samples, as well as the distribution over the magnetic substates. The ionization rate coefficient is particularly sensitive to the density in the sample. It must be checked carefully if frequency drifts of the probe laser light or stray magnetic fields are small enough to avoid incomplete absorption, which would result in underestimation of the density and overestimation of the ionization rate coefficients. If the number of trapped atoms is obtained from fluorescence imaging [11], an accurate calibration of the CCD chip is crucial. Furthermore, collisions of trapped atoms with background atoms or atoms from the atomic beam must be considered. If the trapped atom number is small ($<10^7$), quadratic ionization becomes small and other (linear) ionization mechanisms possibly play a part, hampering accurate measurements. Finally, it should be noted that in most experiments [8,10,11] the magnetic substate distribution has not been taken into account.

It would be interesting to extend the work presented here to trapped samples containing both isotopes and study heteronuclear ionizing collisions. In the case of collisions between distinguishable particles, quantum-statistical symmetry requirements should be absent, which could be confirmed from an investigation of ionizing collisions. This work is in progress in our laboratory. Another interesting extension of the work presented here, is the study of the ionization rates for samples with a prepared substate population. It might be possible to study depolarization due to collisions [15]. Finally, ionizing collisions can also be investigated in the

quantum degenerate regime [62]. Ionization rates could be used to study quantum statistical properties of a quantum-degenerate mixture with high spatial and temporal resolution. It is conceivable that phase separation in a quantum-degenerate mixture will be observable through the ionization rate in the sample.

ACKNOWLEDGMENTS

We thank Jacques Bouma for technical support and Elmar Reinhold for discussions on molecular physics. This work was supported by the Space Research Organization Netherlands (SRON), Grant No. MG-051, and the European Union, Grant No. HPRN-CT-2000-00125.

[1] P. L. Gould, P. D. Lett, P. S. Julienne, W. D. Phillips, H. R. Thorsheim, and J. Weiner, Phys. Rev. Lett. **60**, 788 (1988).
[2] M. Prentiss, A. Cable, J. E. Bjorkholm, S. Chu, E. L. Raab, and D. E. Pritchard, Opt. Lett. **13**, 452 (1988).
[3] J. Weiner, *Cold and Ultracold Collisions in Quantum Microscopic and Mesoscopic Systems* (Cambridge University Press, Cambridge, U.K., 2003).
[4] K. Burnett, P. S. Julienne, P. D. Lett, E. Tiesinga, and C. J. Williams, Nature (London) **416**, 225 (2002).
[5] R. J. W. Stas, J. M. McNamara, W. Hogervorst, and W. Vassen, Phys. Rev. Lett. **93**, 053001 (2004).
[6] K.-A. Suominen, J. Phys. B **29**, 5981 (1996).
[7] F. Bardou, O. Emile, J.-M. Courty, C. I. Westbrook, and A. Aspect, Europhys. Lett. **20**, 681 (1992).
[8] H. C. Mastwijk, J. W. Thomsen, P. van der Straten, and A. Niehaus, Phys. Rev. Lett. **80**, 5516 (1998).
[9] H. C. Mastwijk, M. van Rijnbach, J. W. Thomsen, P. van der Straten, and A. Niehaus, Eur. Phys. J. D **4**, 131 (1998).
[10] P. J. J. Tol, N. Herschbach, E. A. Hessels, W. Hogervorst, and W. Vassen, Phys. Rev. A **60**, R761 (1999).
[11] M. Kumakura and N. Morita, Phys. Rev. Lett. **82**, 2848 (1999).
[12] M. Kumakura and N. Morita, Appl. Phys. B: Lasers Opt. **70**, 555 (2000).
[13] A. Browaeys, J. Poupard, A. Robert, S. Nowak, W. Rooijakkers, E. Arimondo, L. Marcassa, D. Boiron, C. I. Westbrook, and A. Aspect, Eur. Phys. J. D **8**, 199 (2000).
[14] F. Pereira Dos Santos, F. Perales, J. Léonard, A. Sinatra, J. Wang, F. S. Pavone, E. Rasel, C. S. Unnikrishnan, and M. Leduc, Eur. Phys. J. D **14**, 15 (2001).
[15] P. J. Leo, V. Venturi, I. B. Whittingham, and J. F. Babb, Phys. Rev. A **64**, 042710 (2001).
[16] V. Venturi, I. B. Whittingham, P. J. Leo, and G. Peach, Phys. Rev. A **60**, 4635 (1999).
[17] V. Venturi and I. B. Whittingham, Phys. Rev. A **61**, 060703 (2000).
[18] P. S. Julienne and F. H. Mies, J. Opt. Soc. Am. B **6**, 2257 (1989).
[19] G. V. Shlyapnikov, J. T. M. Walraven, U. M. Rahmanov, and M. W. Reynolds, Phys. Rev. Lett. **73**, 3247 (1994).
[20] P. O. Fedichev, M. W. Reynolds, U. M. Rahmanov, and G. V. Shlyapnikov, Phys. Rev. A **53**, 1447 (1996).
[21] N. Herschbach, P. J. J. Tol, W. Hogervorst, and W. Vassen, Phys. Rev. A **61**, 050702(R) (2000).
[22] A. J. Yencha, in *Electron Spectroscopy: Theory, Techniques and Applications*, edited by C. R. Brundle and A. D. Baker (Academic Press, London, 1984), Vol. 5, pp. 197–373.
[23] O. Sirjean, S. Seidelin, J. Viana Gomes, D. Boiron, C. I. Westbrook, A. Aspect, and G. V. Shlyapnikov, Phys. Rev. Lett. **89**, 220406 (2002).
[24] H. S. W. Massey, E. H. S. Burhop, and H. B. Gilbody, *Electronic and Ionic Impact Phenomena* (Oxford University Press, Oxford, 1971), Vol. 3.
[25] J. C. Hill, L. L. Hatfield, N. D. Stockwell, and G. K. Walters, Phys. Rev. A **5**, 189 (1972).
[26] A. Robert, O. Sirjean, A. Browaeys, J. Poupard, S. Nowak, D. Boiron, C. I. Westbrook, and A. Aspect, Science **292**, 461 (2001).
[27] F. Pereira Dos Santos, J. Léonard, J. Wang, C. J. Barrelet, F. Perales, E. Rasel, C. S. Unnikrishnan, M. Leduc, and C. Cohen-Tannoudji, Phys. Rev. Lett. **86**, 3459 (2001).
[28] A. S. Tychkov, T. Jeltes, J. M. McNamara, P. J. J. Tol, N. Herschbach, W. Hogervorst, and W. Vassen, Phys. Rev. A **73**, 031603 (2006).
[29] M. R. Doery, E. J. D. Vredenbregt, S. S. Op de Beek, H. C. W. Beijerinck, and B. J. Verhaar, Phys. Rev. A **58**, 3673 (1998).
[30] H. Katori, H. Kunugita, and T. Ido, Phys. Rev. A **52**, R4324 (1995).
[31] C. Orzel, M. Walhout, U. Sterr, P. S. Julienne, and S. L. Rolston, Phys. Rev. A **59**, 1926 (1999).
[32] H. A. Bethe, Phys. Rev. **47**, 747 (1935).
[33] E. P. Wigner, Phys. Rev. **73**, 1002 (1948).
[34] P. S. Julienne, A. M. Smith, and K. Burnett, Adv. At., Mol., Opt. Phys. **30**, 141 (1993).
[35] F. H. Mies and M. Raoult, Phys. Rev. A **62**, 012708 (2000).
[36] C. Cohen-Tannoudji, B. Diu, and F. Laloë, *Quantum Mechanics* (John Wiley & Sons, New York, 1977).
[37] J. Dalibard, in *Bose-Einstein Condensation in Atomic Gases, Proceedings of the International School of Physics "Enrico Fermi"*, edited by M. Inguscio, S. Stringari, and C. E. Wieman (IOS Press, Amsterdam, 1999), pp. 321–349.
[38] M. W. Müller, A. Merz, M.-W. Ruf, H. Hotop, W. Meyer, and M. Movre, Z. Phys. D: At., Mol. Clusters **21**, 89 (1991).
[39] L. D. Landau and E. M. Lifshitz, *Quantum Mechanics—Non-Relativistic Theory*, 2nd ed. (Pergamon Press, London 1965).
[40] Z.-C. Yan and J. F. Babb, Phys. Rev. A **58**, 1247 (1998).
[41] D. Spelsberg and W. Meyer, J. Chem. Phys. **99**, 8351 (1993).
[42] C. J. Joachain, *Quantum Collision Theory* (North-Holland, Amsterdam, 1975).
[43] J. Kim, S. Moal, M. Portier, J. Dugué, M. Leduc, and C. Cohen-Tannoudji, Europhys. Lett. **72**, 548 (2005).
[44] A. S. Dickinson, F. X. Gadéa, and T. Leininger, J. Phys. B **37**, 587 (2004).
[45] A. Messiah, *Quantum Mechanics—Two Volumes Bound as One* (Dover Publications, Mineola, NY, 1999).
[46] L. E. Ballentine, *Quantum Mechanics—A Modern Development* (World Scientific, Singapore, 1998).
[47] J. P. Burke, Jr., Ph.D. thesis, University of Colorado, 1999 (unpublished).

[48] S. D. Rosner and F. M. Pipkin, Phys. Rev. A **1**, 571 (1970).
[49] A. S. Davydov, *Quantum Mechanics* (Pergamon Press, London, 1965).
[50] R. J. W. Stas, Ph.D. thesis, Vrije Universiteit Amsterdam, 2005 (unpublished).
[51] R. N. Zare, *Angular Momentum: Understanding Spatial Aspects in Chemistry and Physics* (John Wiley & Sons, New York, 1988).
[52] E. E. Nikitin and S. Ya. Umanskii, *Theory of Slow Atomic Collisions* (Springer-Verlag, Berlin, 1984).
[53] P. E. Siska, Rev. Mod. Phys. **65**, 337 (1993).
[54] N. Herschbach, Ph.D. thesis, Vrije Universiteit Amsterdam, 2003 (unpublished).
[55] J. C. J. Koelemeij, A. S. Tychkov, T. Jeltes, W. Hogervorst, and W. Vassen, J. Phys. B **37**, 3501 (2004).
[56] D. Vrinceanu and H. R. Sadeghpour, Phys. Rev. A **65**, 062712 (2002).
[57] H. C. Mastwijk, Ph.D. thesis, Universiteit Utrecht, 1997 (unpublished).
[58] E. W. Rothe, R. H. Neynaber, and S. M. Trujillo, J. Chem. Phys. **42**, 3310 (1965).
[59] D. W. Martin, C. Weiser, R. F. Sperlein, D. L. Bernfeld, and P. E. Siska, J. Chem. Phys. **90**, 1564 (1989).
[60] T. P. Parr, D. M. Parr, and R. M. Martin, J. Chem. Phys. **76**, 316 (1982).
[61] M. Yamazaki, S. Maeda, N. Kishimoto, and K. Ohno, Chem. Phys. Lett. **355**, 311 (2002).
[62] S. Seidelin, J. Viana Gomes, R. Hoppeler, O. Sirjean, D. Boiron, A. Aspect, and C. I. Westbrook, Phys. Rev. Lett. **93**, 090409 (2004).